Supplemental Data

Transcellular Diapedesis Is Initiated

by Invasive Podosomes

Christopher V. Carman, Peter T. Sage, Tracey E. Sciuto, Miguel A. de la Fuente, Raif S. Geha, Hans D. Ochs, Harold F. Dvorak, Ann M. Dvorak, and Timothy A. Springer

Supplemental Experimental Procedures

Antibodies and Reagents

Antibodies to human αL (TS2/4), β2 (CBR-LFA1/7 and CBR-LFA1/2) and ICAM-1 (CBR-IC1/11) have been described (Carman et al., 2003). Anti-VE-cadherin (clone 55-7H1) was from BD Pharmingen (San Diego, CA). Monoclonal anti-PECAM-1 (clone 9G11), polyclonal anti-JAM1 and IL-2 were from R&D Systems (Minneapolis, MN). PECAM-1 function-blocking mAb HEC7 was from RDI (Valhalla, NY). Anti-WASP mAb B9 was from Santa Cruz (CA), while anti-actin mAb was from Chemicon (Temecula, CA). Rabbit polyclonal anti-sera to talin-1 was a generous gift from Dr. K. Burridge (University of North Carolina). Antibody conjugation to Cy3, Cy5 (Amersham, Piscataway, NJ) or Alexa488 (Molecular Probes, Carlsbad, CA) bis-reactive dyes were according to manufacturer's instructions. BAPTA-AM and NEM were from Sigma (St. Louis, MO). ER-Tracker Green and Lyso-Tracker Green were from Molecular Probes. Phytohaemagglutinin (PHA) was from Remel (Lenexa, KS). PP2 was from Calbiochem (San Diego, CA).

Culture of Model Memory Lymphocytes

Preparation of IL-15-cultured primary human lymphocytes (models for memory type lymphocytes (Weninger et al., 2001)) was as described (Shimaoka et al., 2006) and included 3 days of activation with PHA (1 μg/ml) followed by 3-6 days of differentiation in the presence of IL-15 (20 ng/ml).

Analysis of Live-Cell Imaging

Lymphocyte lateral migration over the endothelium was analyzed by manually tracing individual cell outlines in successive video frames, followed by plotting a line connecting the centroids of these outlines. The length of the line was divided by time interval during which it was recorded to calculate average migration velocity.

As a readout for podosome formation, we quantified the time-averaged number of podoprints formed under individual spread and migrating lymphocytes (the podoprint index). For this, podoprints formed under individual lymphocytes were counted in sequential video frames over the interval in which the lymphocyte was adherent and within the field of view. The total number of podoprints was then divided by the number of frames within the interval.

To compare relative enrichment of molecules within podoprints, we employed Pearson's correlation analysis (a statistical test for a linear relationship between two variables in which values of 1 and –1 reflect perfect positive or negative correlation, respectively, and 0 indicates no correlation). For imaging, the two variables are the fluorescence intensities of two distinct fluorophores, which are correlated on a pixel-by-pixel basis. The signal intensity of memb-RFP (to monitor podoprints) was compared to that of various GFP-labeled molecules within endothelial cells. Video frames from live-cell imaging experiments were tightly cropped around regions where clusters of podoprints formed at some point during the duration of an imaging experiment. Sets of at least three successive frames with podosomes present ("podosome-positive") and three successive frames from time points prior to podoprint formation ("podosome-negative") were selected. For each frame, pixel-by-pixel green and red channel intensities were compared, using Volocity software, to generate a Pearson's coefficient. Similar sets of Pearson's coefficients were obtained for at least five distinct podosome clusters (each corresponding to a distinct lymphocyte). The sum of all podosome-negative and all podosome-positive coefficients (at least 15 values for each) were each averaged.

Quantitation of Ultrastructure

Since lymphocyte protrusions that had breached the endothelium completely were extremely heterogeneous in size and shape, we limited our analysis to those protrusions that had not yet breached the endothelium. As the protrusion angles relative to the cross section cannot be known, we could not measure protrusion length, *per se*. Instead, for consistency, we measured the depth of each protrusion, from its base to its distal end, along the axis perpendicular to the plane of the endothelium as defined under "Transmission Election Microscopy" in Experimental Procedures. Endothelial thickness immediately adjacent to each projection was also measured in a similar manner. In addition, analysis of the overall thickness (not specifically related to site of lymphocyte protrusion) of in vitro endothelial monolayers (as well as of guinea pig dermal venular endothelium) was accomplished by taking the average from (at least 50) thickness measurements made at regular intervals along the length of the endothelium from randomly selected representative micrographs. Lymphocyte protrusion width measurements were taken across the location that represented 50% of the total depth.

Total endothelial vesicles were counted within a depth 500 nm from the apical endothelial surface in 500 nm horizontal intervals in micrographs without

lymphocytes or with lymphocytes but lacking protrusions. In micrographs containing protrusions measurements were made 500 nm to the left and the right of the protrusion center. Individual vesicles were identified as being apparently free in the cytoplasm or fused/docked with the apical plasma membrane. Measurements were taken from no less than 74 intervals from micrographs of randomly selected sections.

Supplemental References

Carman, C.V., and Springer, T.A. (2004). A transmigratory cup in leukocyte diapedesis both through individual vascular endothelial cells and between them. J. Cell Biol. *167,* 377–388.

Carman, C.V., Jun, C.-D., Salas, A., and Springer, T.A. (2003). Endothelial cells proactively form microvilli-like membrane projections upon ICAM-1 engagement of leukocyte LFA-11. J. Immunol. *171*, 6135–6144.

Evans, J.G., Correia, I., Krasavina, O., Watson, N., and Matsudaira, P. (2003). Macrophage podosomes assemble at the leading lamella by growth and fragmentation. J. Cell Biol. *161*, 697–705.

Shimaoka, M., Kim, M., Cohen, E. H., Yang, W., Astrof, N., Peer, D., Salas, A., Ferrand, A., and Springer, T. A. (2006). AL-57, a ligand-mimetic antibody to integrin LFA-1, reveals chemokine-induced affinity upregulation in lymphocytes. Proc Natl Acad Sci U S A *103*, 13991-13996.

Weninger, W., Crowley, M.A., Manjunath, N., and von Andrian, U.H. (2001). Migratory properties of naive, effector, and memory CD8(+) T cells. J. Exp. Med. *194*, 953–966.

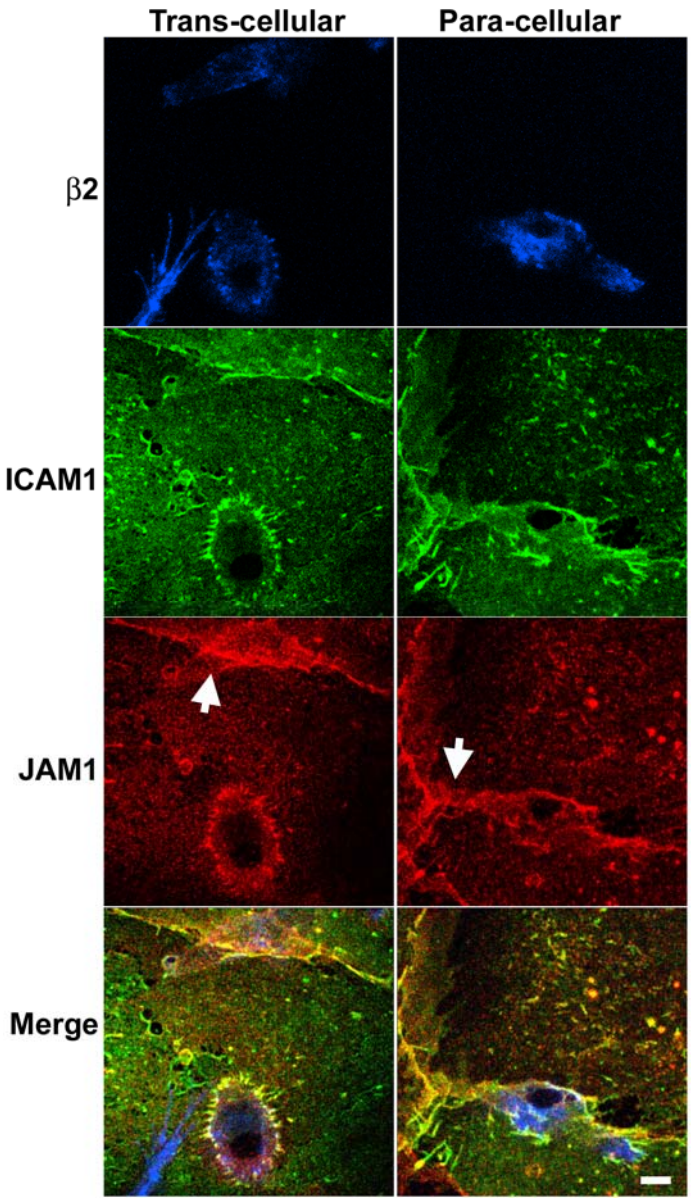

Figure S1. Association of JAM-1 with Both Trans- and Paracellular Diapedesis

Lymphocytes were incubated with TNF-α-activated HLMVEC for 10 minutes followed by fixation, staining for leukocyte integrin β2, ICAM-1 and JAM-1 and confocal microscopy as described in *Experimental Procedures*. Images are Z-stack projections of representative trans- (left panels) and para-cellular (right panels) diapedesis events. Arrows indicate the JAM-1-enriched inter-endothelial junctions. Bar represents 5 μm.

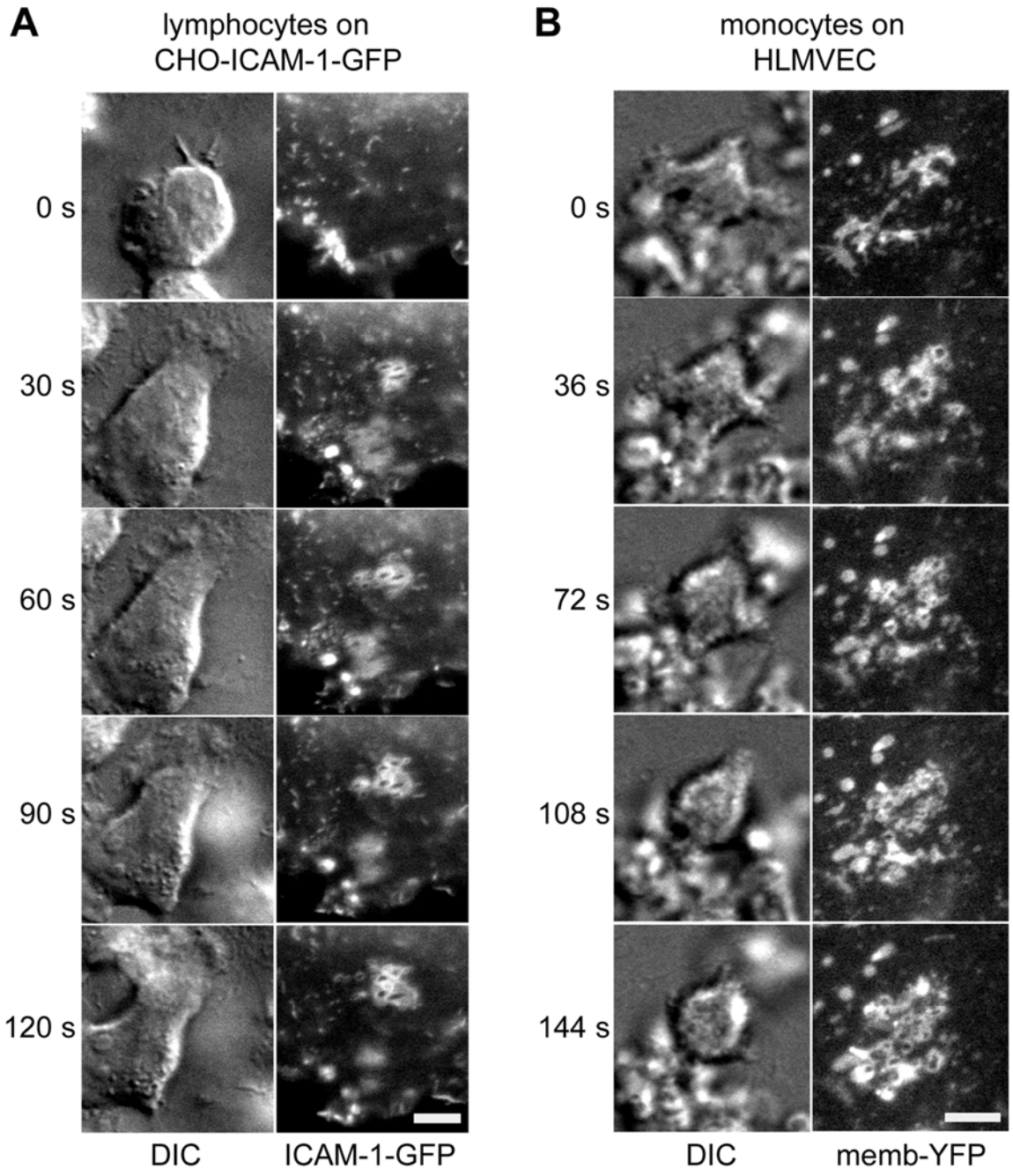

Figure S2. Podoprint Formation on CHO-K1 Cells

A. Lymphocytes induce micron-scale invaginations on the surface of CHO-K1 cells expressing ICAM-1-GFP. A monolayer of CHO-K1 cells stably expressing ICAM-1-GFP (Carman et al., 2003) was pre-incubated with SDF-1 (50 ng/ml, 20 min at 37^{o}C) before washing, addition of lymphocytes and live-cell imaging. Left panels show sequential DIC images (at 30 second intervals, as indicated) depicting a single lymphocyte migrating over the surface of a CHO-K1 cell. Right panels show the corresponding ICAM-1-GFP fluorescence image for

each time point. Note that dynamic micron-scale rings form in clusters on the CHO-K1 cell surface that are essentially identical to those seen on endothelial cells (see Fig.2 and 3). **B. Monocytes induce micro-scale invaginations on the surface of endothelial cells.** TNF-α-activated HLMVEC transiently transfected with memb-YFP (green) were subjected to live-cell imaging upon addition and co-incubation with freshly isolated human monocytes. Left panels are sequential DIC images (at 36 second intervals, as indicated) showing one spreading monocyte and several other clustered monocytes on the endothelium. Right panels are the corresponding endothelial memb-YFP fluorescence images for each time point. Note that the ring-shaped structures formed under the spreading monocyte are essentially identical to those seen under lymphocytes (Fig.2 and 3). Scale bars represent 5 μm.

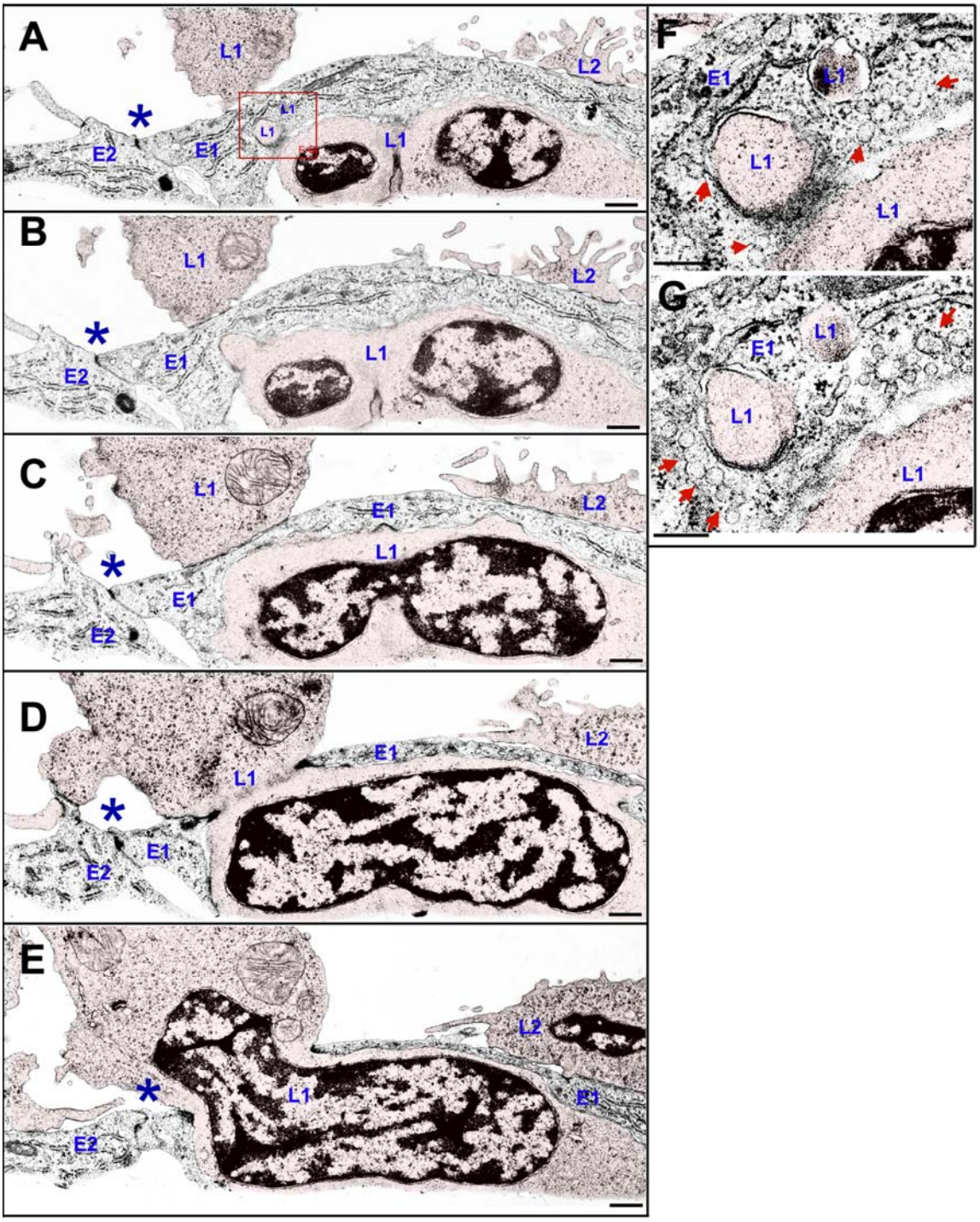

Figure S3. Transmission EM of Lymphocyte Transcellular Diapedesis
Lymphocytes migrating on HDMVEC were fixed after a 10 minute co-incubation and processed for TEM as described in *Experimental Procedures*. In all panels lymphocyte cell area is indicated by a 5% opacity red overlay. A-E. Selected thin (90 nm) sections from a series depict a lymphocyte ("L1") in the process of trans-cellular diapedesis through an individual endothelial cell ("E1"). An endothelial adherens and tight junction (asterisk) with a neighboring endothelial cell ("E2") is

visible and intact in all of 19 sections. In section A-C portions of the lymphocyte are visible both above and below an increasingly attenuated region of endothelium. In section A two small regions of L1 appear "encapsulated" within E1 (Boxed region, see F and G, below). The following sections (B-E) reveal that, in fact, these regions are continuous with the rest of the lymphocyte and represents a cross-section of a peripheral portion of the trans-cellular pore. In sections D and E the open trans-cellular pore is fully apparent. F-G. A magnified region of the periphery of the trans-cellular pore is shown (F shows the boxed region in section A. G shows the same region in a section adjacent to A). Note the enrichment of vesicles and VVO (arrows), both in close proximity and, indeed, apparently fused/docked to (see left-most arrow in F) this trans-cellular pore. Scale bars represent 5 μm (A-D) or 2 μm F-G.

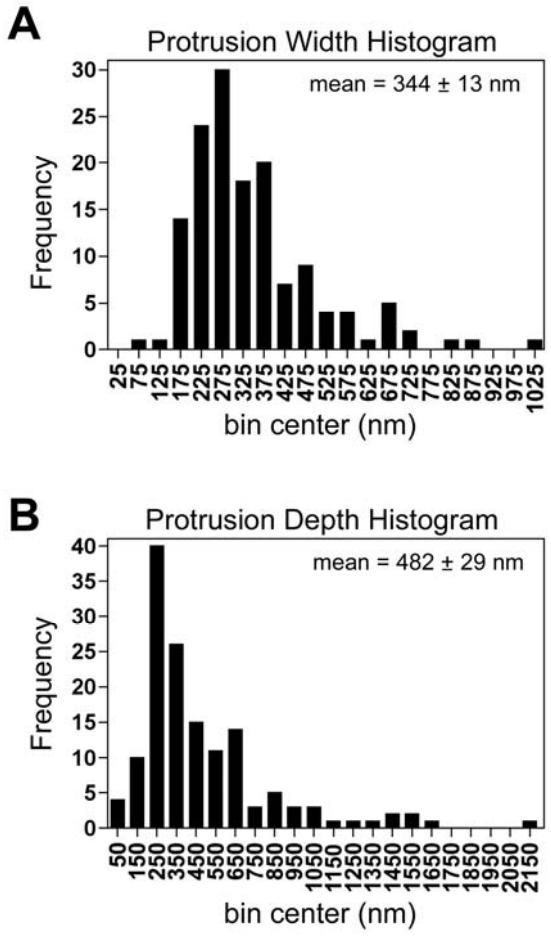

Figure S4. Dimensions of lymphocyte protrusive structures. The width (A) and depth (in the plane normal to that of the endothelium) (B) dimensions of 143 lymphocyte protrusions, described in Fig.5A-D, were measured from micrographs of randomly selected sections. Measurements were binned in 50 (A) or 100 (B) nm increments and the number of measurements within indicated bins plotted as histograms. Mean protrusion width was 344 ± 13 nm. Mean protrusion depth was 482 ± 29 nm. Average overall endothelial thickness (made from measurements at regular intervals independently of protrusion location in randomly selected micrographs) was 1028 ± 277 (ranging from 207 to 2415). Note that these values were similar to those made *in vivo* of guinea pig dermal post capillary venules (related to Fig.5E and F; mean thickness of 933 ± 76 nm, ranging from 165 to 2480). Mean endothelial cell thickness immediately adjacent to sites of podosome protrusion was 1668 nm ± 117 (ranging from 136 to 5766 nm). For consistency this analysis excluded protrusions that had already breached the endothelium. Thus, we speculate that the bias of the non-breaching protrusions toward relatively thicker endothelial regions reflects relatively lower efficiency of endothelial breaching at these locations.

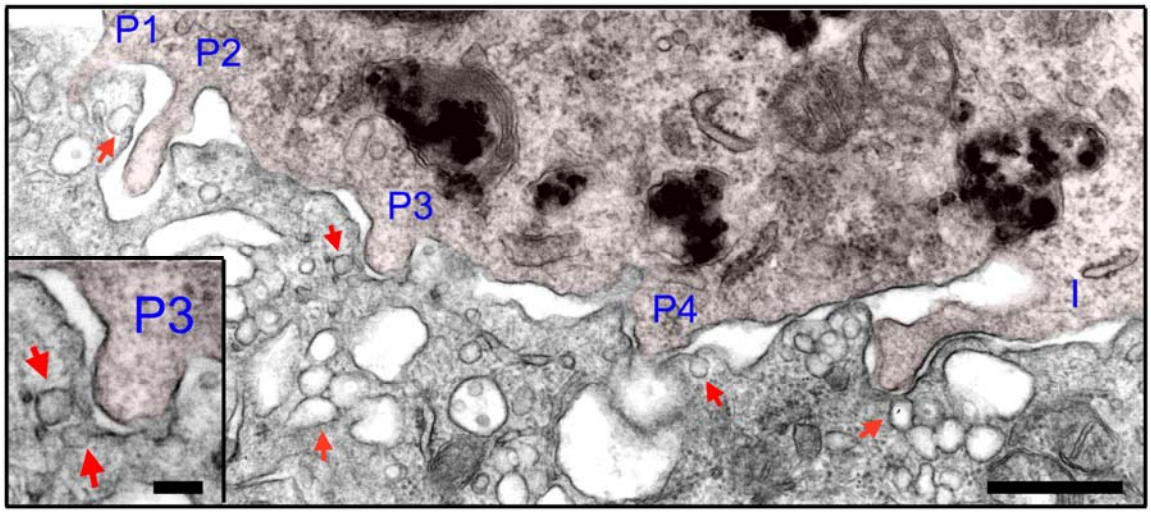

Figure S5. In Vivo Ultrastructure of Murine Mononuclear Cell Podosomes and Invasive Podosomes

MOT tumor tissues were prepared from C3HebFeJ mice injected with colloidal carbon and processed for EM as described in *Experimental Procedures*. A representative murine mononuclear cell (indicated by a 5% opacity red overlay) attached to the tumor vasculature is shown. Podosomes ("P1-P4") and invasive podosomes (I) project into the endothelial surface of tumor associated vessel. Inset shows an expanded view of "P3". Arrows indicate endothelial vesicles and VVOs, both apparently free in the cytoplasm and fused to the plasma membrane, enriched near the mononuclear cell protrusions. Scale bar represents 500 nm (inset shows 100 nm).

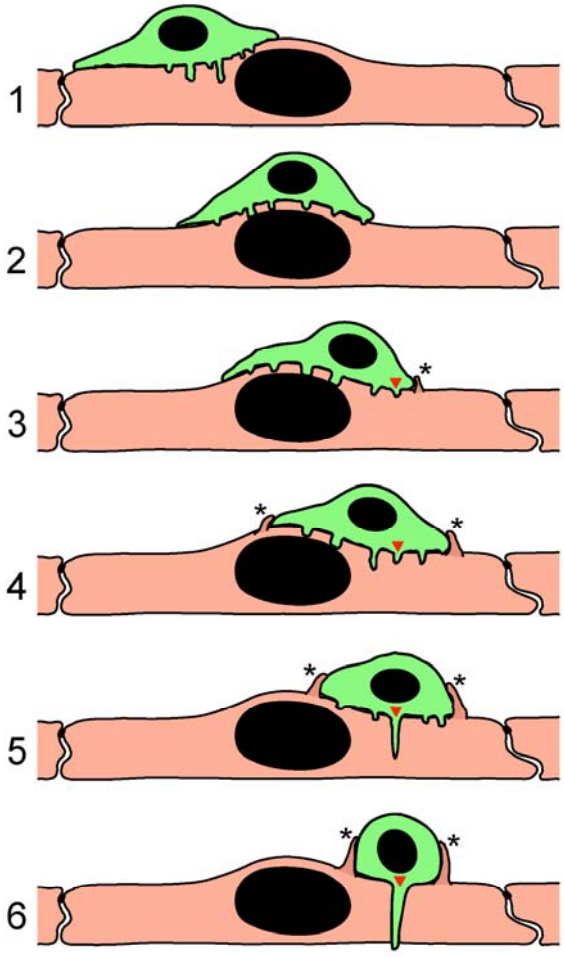

Figure S6. Schematic of Leukocyte Podosome Palpation Behavior
A leukocyte (green) is depicted in the process of lateral migration over, and trans-cellular diapedesis through, an endothelial monolayer (pink). Numbered panels show successive time points that are intended to represent intervals of ~30-60 seconds. Dynamic insertion (~0.2-1 μm in depth) and retraction of multiple podosomes into the apical surface of the endothelium is shown as lateral migration proceeds (panels 1-4). Podosomes formed over the endothelial nucleus (large black oval) are impeded by resistance from the nuclear lamina and remain shallow (panels 2-4). At a location of sufficiently low endothelial resistance an "invasive podosome" (red arrow heads) progressively extends several microns in depth to ultimately breach the endothelium trans-cellularly (panels 3-6). Also depicted is the previously described (Carman and Springer, 2004) and distinct "transmigratory cup" structure (asterisks). The transmigratory cup consists of vertical microvilli-like projections (rich in actin, ICAM-1, VCAM-1 (Carman and Springer, 2004), as well as PECAM-1 (Fig.1D) and JAM-1 (Fig.S1)) that are formed proactively by the endothelium and surround the periphery of adherent leukocytes. These structures seem to corral leukocytes, guide diapedesis and provide a vertical traction substrate for protrusion of leukocytes against the endothelial surface.